Opto-Electronic Science

Supplementary information
2022, Vol. 1, No. 4

DOI: 10.29026/oes.2022.210005

Charge carrier dynamics in different crystal phases of $CH_3NH_3PbI_3$ perovskite

Efthymis Serpetzoglou[1*], Ioannis Konidakis[1], George Kourmoulakis[1,3], Ioanna Demeridou[1,4], Konstantinos Chatzimanolis[2], Christos Zervos[2], George Kioseoglou[1,3], Emmanuel Kymakis[2] and Emmanuel Stratakis[1,3,4*]

[1]Institute of Electronic Structure and Laser (IESL), Foundation for Research and Technology-Hellas (FORTH), Herakleio 70013, Greece; [2]Center of Materials Technology and Photonics, Electrical and Computer Engineering Department, Hellenic Mediterranean University, Herakleio 71004, Greece; [3]Department of Materials Science and Technology, University of Crete, Herakleio 70013, Greece; [4]Department of Physics, University of Crete, Herakleio 70013, Greece.

*Correspondence: E Serpetzoglou, E-mail: eserpe@iesl.forth.gr; E Stratakis, E-mail: stratak@iesl.forth.gr

This file includes:

Section 1: Additional measurements
Section 2: Temperature-dependent time-resolved absorption spectroscopy
Section 3: TAS error fitting analysis

Supplementary information for this paper is available at https://doi.org/10.29026/oes.2022.210005

Section 1: Additional measurements

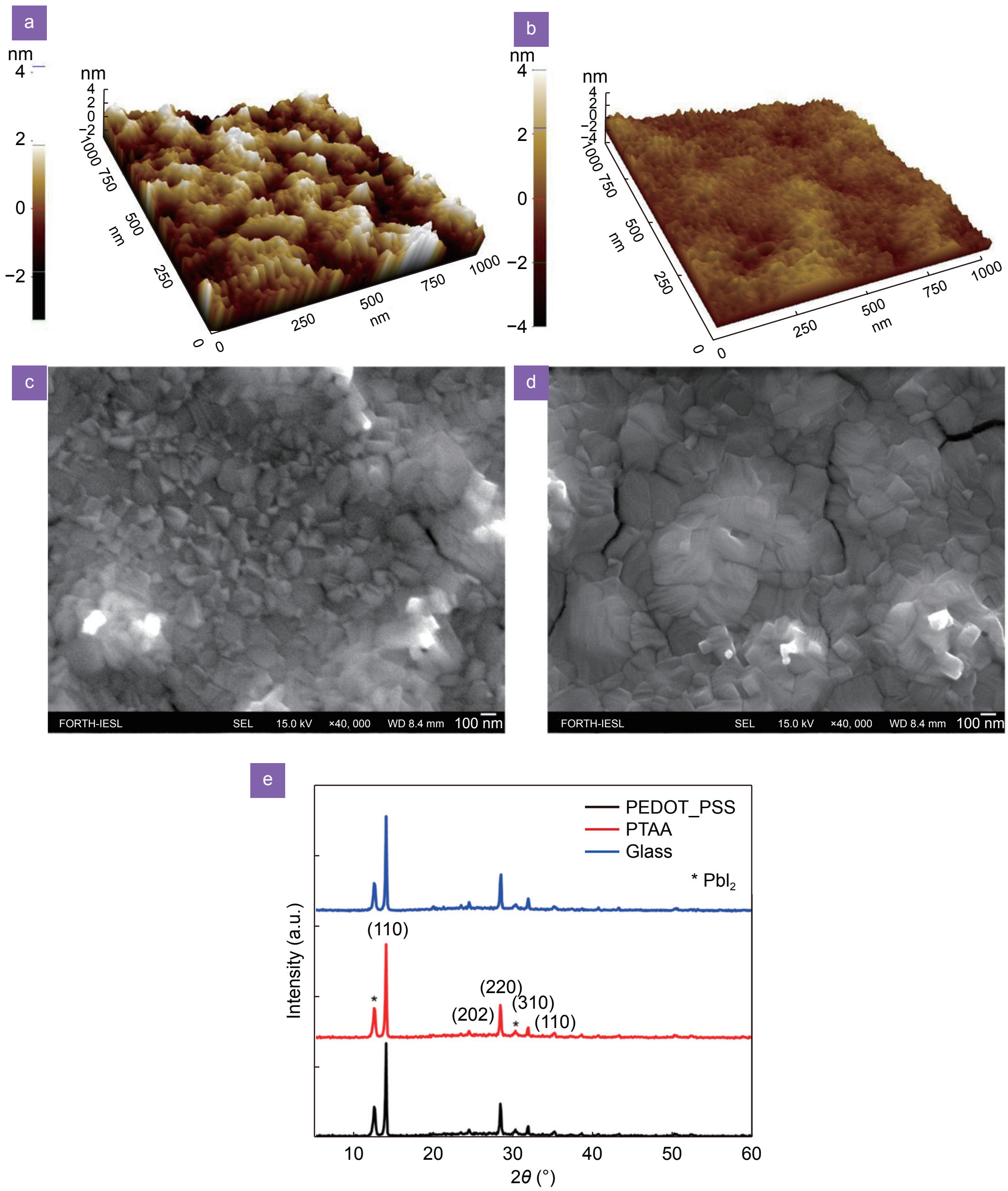

Fig. S1 | Atomic force microscopy (AFM) surface profiles of (**a**) PEDOT:PSS and (**b**) PTAA polymers prior to $CH_3NH_3PbI_3$ perovskite deposition. Scanning electron microscopy (SEM) photos of the $CH_3NH_3PbI_3$ perovskite structure grown on (**c**) PEDOT:PSS and (**d**) PTAA hole transport layers and (**e**) the XRD pattern for all studied architectures. Taken from ref.[2], except the XRD pattern for Glass/$CH_3NH_3PbI_3$ configuration in (e).

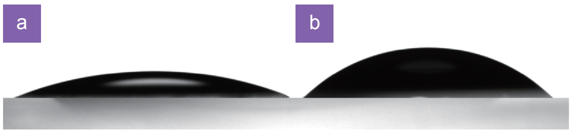

Fig. S2 | Photographs of the shape of a 5 μL de-ionized water droplet on PEDOT:PSS (**a**) and PTAA (**b**) polymer substrates that provide the corresponding contact angles. Taken from ref.[2].

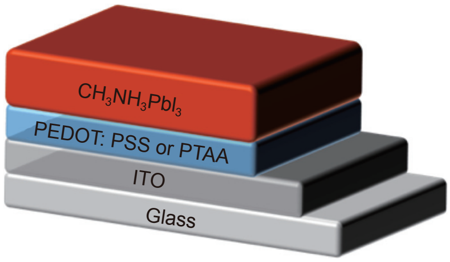

Fig. S3 | Perovskite/HTL architecture components that used for TAS measurements.

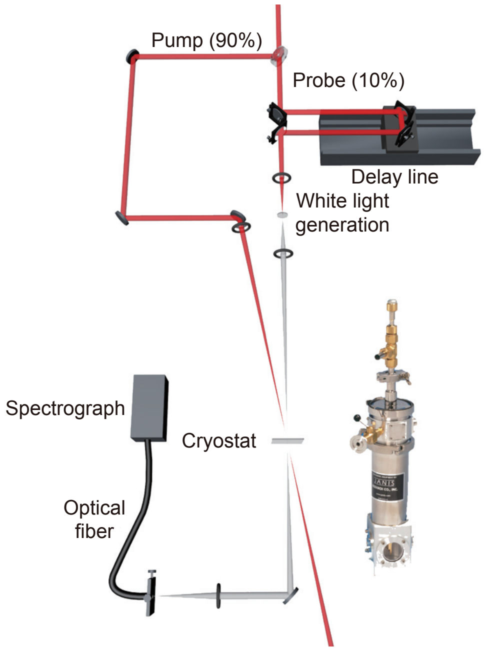

Fig. S4 | Schematic representation of Newport Transient Absorption Spectrometer (TAS-1) and the cryostat that used for the low temperatures TAS measurements.

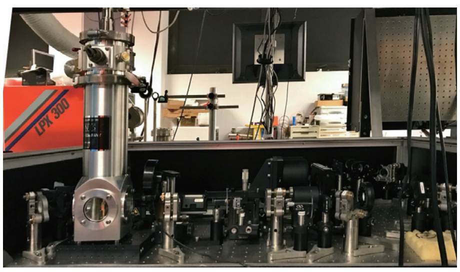

Fig. S5 | Janis VPF-100 cryostat, integrated into the TAS setup.

Section 2: Temperature-dependent time-resolved absorption spectroscopy

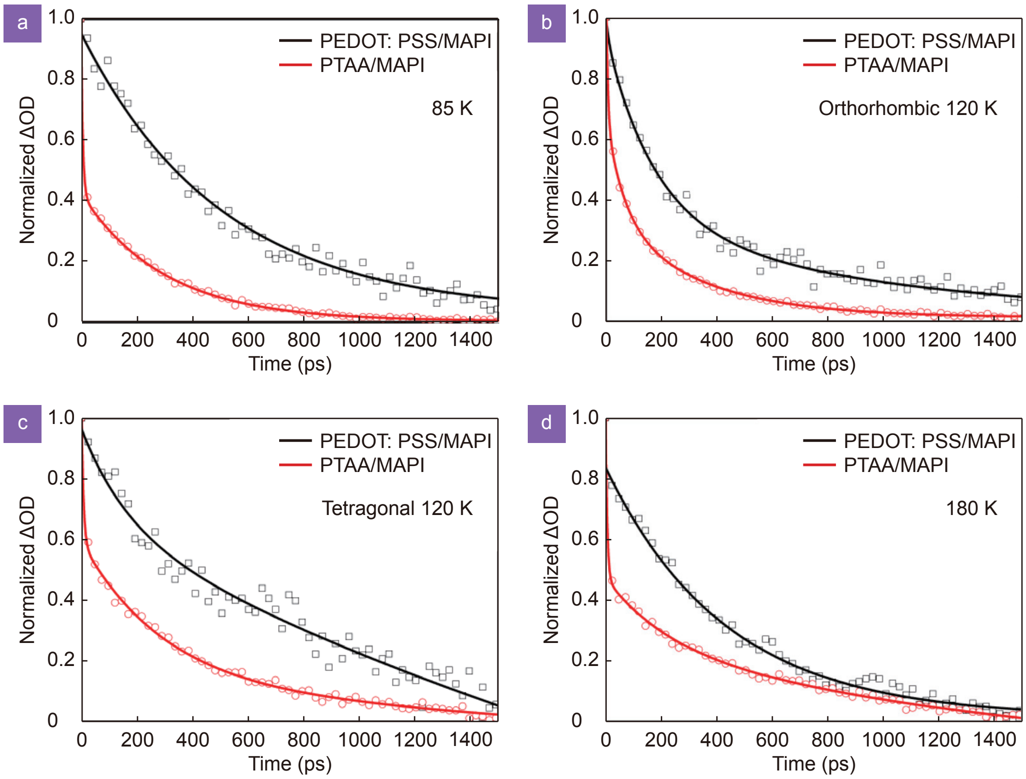

Fig. S6 | Normalized optical density (ΔOD) vs delay time for PEDOT:PSS/$CH_3NH_3PbI_3$ and PTAA/$CH_3NH_3PbI_3$ configurations for the orthorhombic phase at (**a**) 85 K, (**b**) 120 K and for the tetragonal phase at (**c**) 120 K and (**d**) 180 K. Symbols present the transient band edge bleach kinetics, while solid lined present the high-order polynomial fitting.

Section 3: TAS error fitting analysis

We choose the appropriate equation and fitting model (ExpDec3) because there are three different phenomena that take place in the solar cell device when it's irradiated by light, the charge carrier trapping (τ_1), the hole injection (τ_2) and the exciton recombination (τ_3). Before we fit our data, we narrow the range of τ_1 and τ_2 and y_0. Specifically, we narrow the time ranges for τ_1, τ_2, from 5 ps up to 30 ps and from 50 ps up to 600 ps, respectively, for both configurations in order to obtain fast and efficient hole injection from the perovskite layer to hole transport layer. Moreover, we narrow also the constant, y_0, of our equation between 0 and the lowest value of ΔOD, because in the time range of our setup is impossible not to have excited electrons in the conduction band of the perovskite layer.

Additionally, in Tables S1, 2 we present the further analysis at 180 K for both configurations for tri-exponential fitting model that we use. We have to mention that the same trend was observed also for 85 K and 120 K for both architectures. Especially, in Tables S1, S2(a) we show the optimum fitting without any fixed term (fitting software internal algorithm provides best fit, only from a mathematical point of view). Tables S1, S2 (b) present the time components in which the y_0 and τ_1 are fixed in the values from the optimum fitting. We obtain that the deviation of τ_2 and τ_3 is within the error that we have already presented in the manuscript. Moreover, Tables S1, S2 (c) show the corresponding fitting when only τ_2 is fixed in the optimum value. With this procedure, we take unrealistic τ_1 and τ_3 for the perovskite solar cell. Finally, in Tables S1, S2 (d, f) we present the time components when the τ_3 is fixed with lower and higher compared with the τ_3 value extracted from the optimum value, respectively. In both cases, the τ_2 value is too slow to present the hole injection from the perovskite to the hole transport layer.

In order to eliminate any doubts about the fitting uncertainties in Table S3, 4 we present the lower and upper limits for each time component for both configurations. In both cases (PEDOT:PSS/$CH_3NH_3PbI_3$ and PTAA/$CH_3NH_3PbI_3$) the errors for the τ_1, τ_2 and τ_3 are 2 ps, 8 ps and 13 ps, respectively. Within these limits, we obtain values for time components that are reasonable for the operation of the perovskite solar cell. Firstly, we initiate an upper and a lower limits

Table S1 | Fitting analysis at 180 K for PEDOT: PSS/$CH_3NH_3PbI_3$ configuration. (a) The optimum fitting. (b) y_0 and τ_1 are fixed. (c) τ_2 is fixed, and (d-f) τ_3 is fixed.

(a)Model	ExpDec3
Equation	$y=A_1\times\exp(-x/\tau_1)+A_2\times\exp(-x/\tau_2)+A_3\times\exp(-x/\tau_3)+y_0$
Plot	DeltaOD
y_0	0.00858±5.48E-4
τ_1	14.7±1.95
τ_2	266±7.85
τ_3	933±12.60
Adj. R-Square	0.9978

(b)Model	ExpDec3
Equation	$y=A_1\times\exp(-x/\tau_1)+A_2\times\exp(-x/\tau_2)+A_3\times\exp(-x/\tau_3)+y_0$
Plot	DeltaOD
y_0	0.009±0
τ_1	14.7±0
τ_2	260±2.79
τ_3	944±9.81
Adj. R-Square	0.9977

(c)Model	ExpDec3
Equation	$y=A_1\times\exp(-x/\tau_1)+A_2\times\exp(-x/\tau_2)+A_3\times\exp(-x/\tau_3)+y_0$
Plot	DeltaOD
y_0	0.0065±0.0029
τ_1	467.2±8.1E5
τ_2	266±0
τ_3	540±7.4E5
Adj. R-Square	0.9971

(d)Model	ExpDec3
Equation	$y=A_1\times\exp(-x/\tau_1)+A_2\times\exp(-x/\tau_2)+A_3\times\exp(-x/\tau_3)+y_0$
Plot	DeltaOD
y_0	0.0072±0.0025
τ_1	45.14±3.2
τ_2	470.9±92.9
τ_3	500±0
Adj. R-Square	0.9977

(e)Model	ExpDec3
Equation	$y=A_1\times\exp(-x/\tau_1)+A_2\times\exp(-x/\tau_2)+A_3\times\exp(-x/\tau_3)+y_0$
Plot	DeltaOD
y_0	0.00838±1.3E-4
τ_1	14.2±1.81
τ_2	269±5.10
τ_3	933±0
Adj. R-Square	0.9978

(f) Model	ExpDec3
Equation	$y=A_1\times\exp(-x/\tau_1)+A_2\times\exp(-x/\tau_2)+A_3\times\exp(-x/\tau_3)+y_0$
Plot	DeltaOD
y_0	0.0059±0.0011
τ_1	38.82±3.35
τ_2	573±85.24
τ_3	1200±0
Adj. R-Square	0.9977

Table S2 | Fitting analysis at 180 K for PTAA/$CH_3NH_3PbI_3$ configuration. (a) The optimum fitting. (b) y_0 and τ_1 are fixed. (c) τ_2 is fixed, and (d–f) τ_3 is fixed.

(a)Model	ExpDec3
Equation	$y=A_1\times\exp(-x/\tau_1)+A_2\times\exp(-x/\tau_2)+A_3\times\exp(-x/\tau_3)+y_0$
Plot	DeltaOD
y_0	0.001287±5.4E-4
τ_1	5.7±1.95
τ_2	57±7.85
τ_3	1839±12.60
Adj. R-Square	0.9978

(b)Model	ExpDec3
Equation	$y=A_1\times\exp(-x/\tau_1)+A_2\times\exp(-x/\tau_2)+A_3\times\exp(-x/\tau_3)+y_0$
Plot	DeltaOD
y_0	0.013±0
τ_1	5.7±0
τ_2	64±5.54
τ_3	1827±10.94
Adj. R-Square	0.9972

(c)Model	ExpDec3
Equation	$y=A_1\times\exp(-x/\tau_1)+A_2\times\exp(-x/\tau_2)+A_3\times\exp(-x/\tau_3)+y_0$
Plot	DeltaOD
y_0	0.0083±0.0029
τ_1	519.7±1.3E5
τ_2	57±0
τ_3	783±7.4E5
Adj. R-Square	0.9973

(d)Model	ExpDec3
Equation	$y=A_1\times\exp(-x/\tau_1)+A_2\times\exp(-x/\tau_2)+A_3\times\exp(-x/\tau_3)+y_0$
Plot	DeltaOD
y_0	0.0069±0.0015
τ_1	45.14±3.2
τ_2	470.9±92.9
τ_3	1200±0
Adj. R-Square	0.9976

(e)Model	ExpDec3
Equation	$y=A_1\times\exp(-x/\tau_1)+A_2\times\exp(-x/\tau_2)+A_3\times\exp(-x/\tau_3)+y_0$
Plot	DeltaOD
y_0	0.001289±1.9E-4
τ_1	5.1±1.81
τ_2	56.8±3.90
τ_3	1839±0
Adj. R-Square	0.9978

(f) Model	ExpDec3
Equation	$y=A_1\times\exp(-x/\tau_1)+A_2\times\exp(-x/\tau_2)+A_3\times\exp(-x/\tau_3)+y_0$
Plot	DeltaOD
y_0	0.0084±0.0021
τ_1	129.22±5.91
τ_2	673±126.91
τ_3	2500±0
Adj. R-Square	0.9970

Table S3 | Lower and upper limits for time components for PEDOT:PSS/$CH_3NH_3PbI_3$ architecture.

	Lower limit	Upper limit
y_0	Fixed at 0.009	
τ_1 (ps)	12.7	16.7
τ_2 (ps)	258	274
τ_3 (ps)	920	946

Table S4 | Lower and upper limits for time components for PTAA/$CH_3NH_3PbI_3$ architecture.

	Lower limit	Upper limit
y_0	Fixed at 0.013	
τ_1 (ps)	3.7	7.7
τ_2 (ps)	49	65
τ_3 (ps)	1826	1852

of τ_1 at values that are physically explainable. The lower and upper limits of τ_1 take values for τ_2 and τ_3. If they are not realistic, we further reduce the upper and lower limits of τ_1, until we reach the value range of τ_1 that gives realistic results for τ_2, τ_3. So, the τ_1 value gives me the error for τ_2 and τ_3 time components. In this way, we have an empirical adaptation that has a physical explanation and is actually shifted.

References

1. Kakavelakis G, Maksudov T, Konios D, Paradisanos I, Kioseoglou G et al. Efficient and highly air stable planar inverted perovskite solar cells with reduced graphene oxide doped PCBM electron transporting layer. *Adv Energy Mater* **7**, 1602120 (2017).
2. Serpetzoglou E, Konidakis I, Kakavelakis G, Maksudov T, Kymakis E et al. Improved carrier transport in perovskite solar cells probed by femtosecond transient absorption spectroscopy. *ACS Appl Mater Interfaces* **9**, 43910–43919 (2017).
3. Konidakis I, Maksudov T, Serpetzoglou E, Kakavelakis G, Kymakis E et al. Improved charge carrier dynamics of $CH_3NH_3PbI_3$ perovskite films synthesized by means of laser-assisted crystallization. *ACS Appl Energy Mater* **1**, 5101–5111 (2018).